

# Valley-polarized quantum anomalous Hall insulator in monolayer RuBr<sub>2</sub>

San-Dong Guo<sup>1</sup>, Wen-Qi Mu<sup>1</sup> and Bang-Gui Liu<sup>2,3</sup>

<sup>1</sup>*School of Electronic Engineering, Xi'an University of Posts and Telecommunications, Xi'an 710121, China*

<sup>2</sup>*Beijing National Laboratory for Condensed Matter Physics, Institute of Physics, Chinese Academy of Sciences, Beijing 100190, People's Republic of China and*

<sup>3</sup>*School of Physical Sciences, University of Chinese Academy of Sciences, Beijing 100190, People's Republic of China*

Coexistence of intrinsic ferrovalley (FV) and nontrivial band topology attracts intensive interest both for its fundamental physics and for its potential applications, namely valley-polarized quantum anomalous Hall insulator (VQAHI). Here, based on first-principles calculations by using generalized gradient approximation plus  $U$  (GGA+ $U$ ) approach, the VQAHI induced by electronic correlation or strain can occur in monolayer RuBr<sub>2</sub>. For perpendicular magnetic anisotropy (PMA), the ferrovalley (FV) to half-valley-metal (HVM) to quantum anomalous Hall (QAH) to HVM to FV transitions can be driven by increasing electron correlation  $U$ . However, there are no special QAH states and valley polarization for in-plane magnetic anisotropy. By calculating actual magnetic anisotropy energy (MAE), the VQAHI indeed can exist between two HVM states due to PMA, a unit Chern number/a chiral edge state and spontaneous valley polarization. The increasing  $U$  can induce VQAHI, which can be explained by sign-reversible Berry curvature or band inversion between  $d_{xy}/d_{x^2-y^2}$  and  $d_{z^2}$  orbitals. Even though the real  $U$  falls outside the range, the VQAHI can be achieved by strain. Taking  $U=2.25$  eV as a concrete case, the monolayer RuBr<sub>2</sub> can change from a common ferromagnetic (FM) semiconductor to VQAHI under about 0.985 compressive strain. It is noted that the edge states of VQAHI are chiral-spin-valley locking, which can achieve complete spin and valley polarizations for low-dissipation electronics devices. Both energy band gap and valley splitting of VQAHI in monolayer RuBr<sub>2</sub> are higher than the thermal energy of room temperature (25 meV), which is key at room temperature for device applications. It is found that electronic correlation or strain have important effects on Curie temperature of monolayer RuBr<sub>2</sub>. These results can be readily extended to other monolayer MXY (M = Ru, Os; X/Y=Cl, Br I). Our works emphasize the importance of electronic correlation and PMA to study FV materials, and provide a pathway to realize VQAHI.

Keywords: Ferrovalley, Band topology, Electronic correlation, Strain

Email:sandongyuwang@163.com

## I. INTRODUCTION

The valleys, namely the extrema on the valence/conduction band, provide a different degree of freedom to manipulate information analogous to charge and spin (called as valleytronics), which has attracted intensive attention<sup>1-7</sup>. The representative valley materials are transition-metal dichalcogenide (TMD) monolayers with the missing inversion symmetry<sup>6</sup>, where two well separated inequivalent valleys can exist, and their energies are degenerate within spin-orbit coupling (SOC) interaction. To take advantage of the valley degree of freedom, the valley polarization should be induced, and several strategies have been proposed, such as the optical pumping, magnetic field, magnetic substrates and magnetic doping<sup>8-11</sup>. However, these methods limits the valleytronics developments due to very weak valley polarization. The time-reversal symmetry of two-dimensional (2D) magnetic semiconductors is naturally broken, which can give rise to spontaneous valley polarization together with the SOC interactions, namely FV material<sup>12</sup>. Many FV materials have been predicted by the density functional theory (DFT) calculations<sup>13-26</sup>. Recently, a new concept of HVM has been proposed<sup>16</sup>, being analogous to half metals in spintronics. The one valley of HVM is metallic, while the other is semiconducting, which possesses 100% valley polarization.

Since the quantum spin Hall (QSH) state is discovered in graphene<sup>27,28</sup>, the QSH materials have attracted tremendous attention. The QSH insulator has a bulk energy gap with topologically protected helical edge states, which are protected by topology and are robust against backscattering. The breaking time-reversal symmetry of 2D topological insulator results in the QAH effect, which can display quantized Hall conductance under zero magnetic field. Experimentally, the QAH insulator is firstly observed in Cr doped (Bi,Sb)<sub>2</sub>Te thin films below 30 mK<sup>29</sup>. A higher-temperature QAH insulator is still a challenge in experiment<sup>29,30</sup>. Recently, some robust QAH insulator are proposed with high Curie temperature<sup>31-33</sup>.

It's a natural idea to combine valleytronics and band topology, namely VQAHI. The valley-polarized quantum anomalous Hall effect (VQAHE) can be realized in the Co decorated In-triangle adlayer on a Si(111) surface<sup>34</sup>, metal-organic frameworks (MOFs)<sup>35</sup>, bilayer graphene with layer-dependent proximity effects<sup>36</sup>, MXenes<sup>37</sup>, bilayer graphene subject interlayer bias and light irradiation<sup>38</sup>. However, it is highly desirable to search for a VQAHI, which is experimentally feasible in 2D materials with simple lattice structure. Recently, the RuBr<sub>2</sub> monolayer with 1H-MoS<sub>2</sub> type structure is predicted to become VQAHI by strain<sup>39</sup>. However, the electronic correlation and magnetic anisotropy are not detailedly taken into account during the calculations of

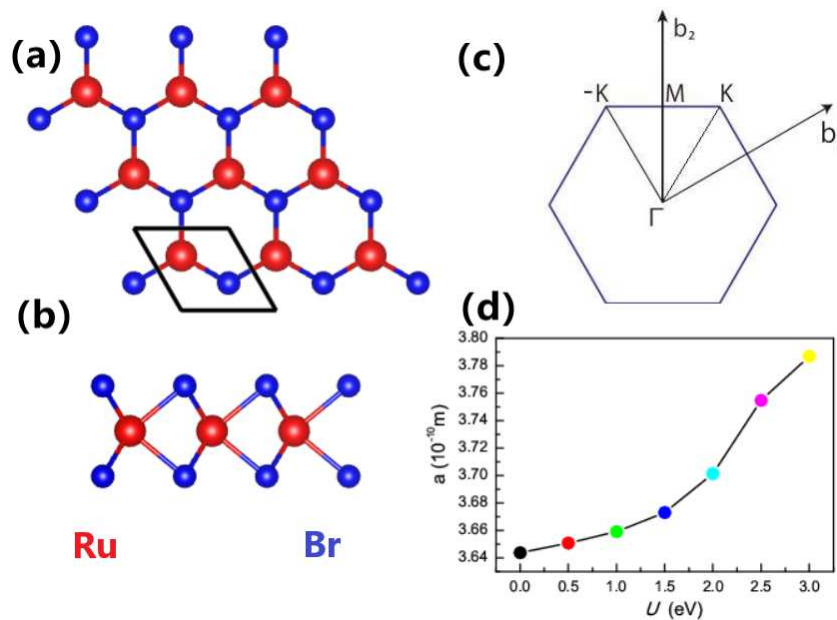


FIG. 1. (Color online) For RuBr<sub>2</sub> monolayer, the (a) top view and (b) side view of crystal structure, and (c) the Brillouin zone with high-symmetry points labeled, and (d) the lattice constants  $a$  as a function of  $U$ .

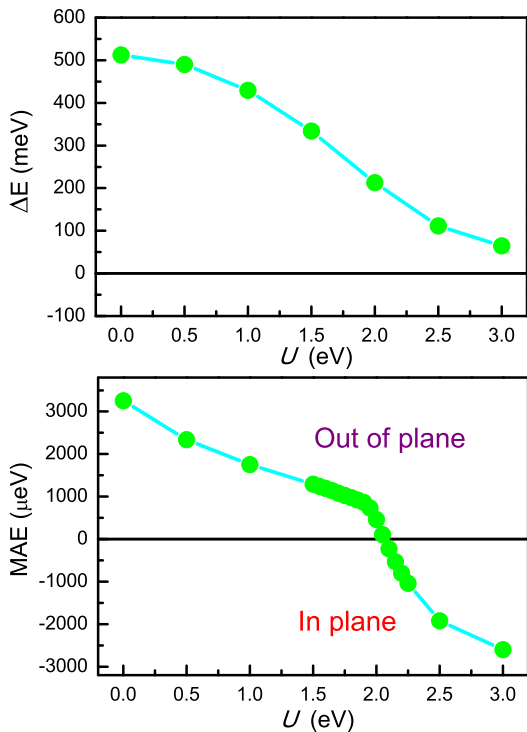


FIG. 2. (Color online) For RuBr<sub>2</sub> monolayer, the energy differences  $\Delta E$  with rectangle supercell between AFM and FM ordering and MAE as a function of  $U$ .

electronic structures, which are very key to produce novel electronic states<sup>16,40,41</sup>. In this work, the electronic correlation and magnetic anisotropy on electronic structures

of RuBr<sub>2</sub> monolayer are comprehensively investigated by using GGA+ $U$ +SOC approach. It is found that different correlation strengths ( $U$ ) along with different magnetic anisotropy (out-of-plane and in-plane) can induce different electronic states. For PMA, the increasing  $U$  can drive the system into FV to HVM to QAH to HVM to FV states. But, there are no novel QAH states and observable valley polarization for in-plane situation. In the appropriate  $U$  range, the RuBr<sub>2</sub> monolayer indeed possesses PMA, QAH states and spontaneous valley polarization, which is a VQAH. Even though the real  $U$  is beyond the scope of achieving VQAH, it can be realized by strain. Our works highlight the importance of correlation effects and magnetic anisotropy in RuBr<sub>2</sub> monolayer.

The rest of the paper is organized as follows. In the next section, we shall give our computational details and methods. In the next few sections, we shall present structure and magnetic properties, electronic correlation and strain effects on electronic properties and Curie temperature of RuBr<sub>2</sub> monolayer. Finally, we shall give our discussion and conclusion.

## II. COMPUTATIONAL DETAIL

We perform spin-polarized first-principles calculations within DFT<sup>42</sup>, as implemented in VASP code<sup>43–45</sup>. The projected augmented wave (PAW) method is adopted, and the GGA of Perdew-Burke-Ernzerhof (PBE-GGA)<sup>46</sup> is used as exchange-correlation potential. The energy cut-off of 500 eV is used to attain accurate results. The total energy convergence criterion of  $10^{-8}$  eV is used, and

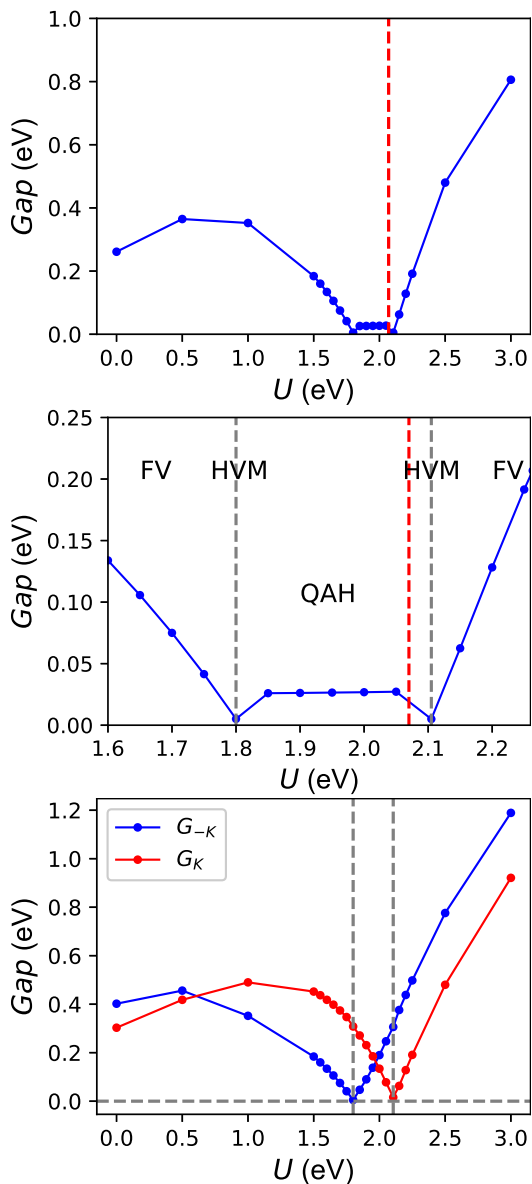


FIG. 3. (Color online) For RuBr<sub>2</sub> monolayer with out-of-plane magnetic anisotropy, the top plane shows global energy band gap as a function of  $U$  (0-3 eV). The middle plane is the enlarged view of the top plane between  $U=1.60$  eV and 2.25 eV, and the phase diagram is shown with different  $U$  region. The bottom plane shows the energy band gaps for the -K and K valleys. The vertical red dotted line means that actual MAE changes from out-of-plane to in-plane.

the force convergence criteria of being less than  $0.0001 \text{ eV} \cdot \text{\AA}^{-1}$  is set on each atom. A vacuum space with a thickness of more than  $18 \text{ \AA}$  is used to ensure decoupling between the periodic layers. The  $\Gamma$ -centered  $24 \times 24 \times 1$  k-mesh is employed to sample the Brillouin zone for structure optimization, electronic structures and elastic properties, and  $12 \times 24 \times 1$  Monkhorst-Pack k-point mesh for FM and antiferromagnetic (AFM) energies with rectangle supercell. The GGA+ $U$  method within the rota-

tionally invariant approach proposed by Dudarev et al is employed to describe the strong correlated Ru- $d$  electrons, where only the effective  $U$  ( $U_{eff}$ ) by subtracting exchange parameters from the on-site Coulomb interaction parameter is meaningful. The SOC effect is explicitly included to investigate MAE, electronic and topological properties of RuBr<sub>2</sub> monolayer.

We use strain-stress relationship (SSR) method to attain elastic stiffness tensor  $C_{ij}$ . The 2D elastic coefficients  $C_{ij}^{2D}$  have been renormalized by  $C_{ij}^{2D} = L_z C_{ij}^{3D}$ , where the  $L_z$  is the length of unit cell along  $z$  direction. The edge states are calculated with the maximal localized Wannier function tight-binding model by employing the  $d$ -orbitals of Ru atoms and the  $p$ -orbitals of Br atoms<sup>47,48</sup>. The Berry curvatures of RuBr<sub>2</sub> monolayer are calculated directly from the calculated wave functions based on Fukui's method<sup>49</sup> by using the VASP-BERRY code<sup>50,51</sup>. We use  $40 \times 40$  supercell and  $10^7$  loops to perform the Monte Carlo (MC) simulations for calculating Curie temperature  $T_C$  of RuBr<sub>2</sub> monolayer, as implemented in Mcsolver code<sup>52</sup>.

### III. STRUCTURE AND MAGNETIC PROPERTIES

The RuBr<sub>2</sub> monolayer possesses  $P\bar{6}m2$  symmetry with space group No.187, which consists Br-Ru-Br sandwich layer, shown in Figure 1 along with Brillouin zone with high-symmetry points. The RuBr<sub>2</sub> monolayer shares the same crystal structure with classical 2D material 1H-MoS<sub>2</sub>. Its inversion symmetry is broken, which can lead to many novel properties, such as piezoelectricity and valley features. Different from the previous works<sup>16,39,40</sup>, we optimize lattice constants  $a$  of RuBr<sub>2</sub> monolayer at different  $U$  (0-3 eV), as illustrated in Figure 1. With increasing  $U$ , the  $a$  increases from  $3.644 \text{ \AA}$  to  $3.787 \text{ \AA}$ . To obtain the magnetic ground states, we calculate the total energy difference between AFM and FM ordering by using rectangle supercell as a function of  $U$ , as plotted in Figure 2. The FM states are found to be the magnetic ground states for all considered  $U$  values, and the increasing  $U$  weakens FM interaction, which has important influence on  $T_C$  of RuBr<sub>2</sub> monolayer. The direction of magnetic anisotropy is very critical to determine topological and valley properties of some 2D materials<sup>40,41</sup>. Here, the MAE is used to determine intrinsic magnetic anisotropy of RuBr<sub>2</sub> monolayer at different  $U$  value by calculating  $E_{MAE} = E_{(100)} - E_{(001)}$  within GGA+SOC+ $U$ , which is shown in Figure 2. The positive  $E_{MAE}$  means out-of-plane magnetic anisotropy, while the negative value suggests the in-plane one. With increasing  $U$ , the magnetic anisotropy direction changes from out-of-plane to in-plane one, and the critical  $U$  value is about 2.07 eV.

The dynamical and thermal stabilities of RuBr<sub>2</sub> monolayer have been proved by phonon spectra without soft modes and the molecular-dynamics simulations<sup>39</sup>. To further check its mechanical stability, the elastic prop-

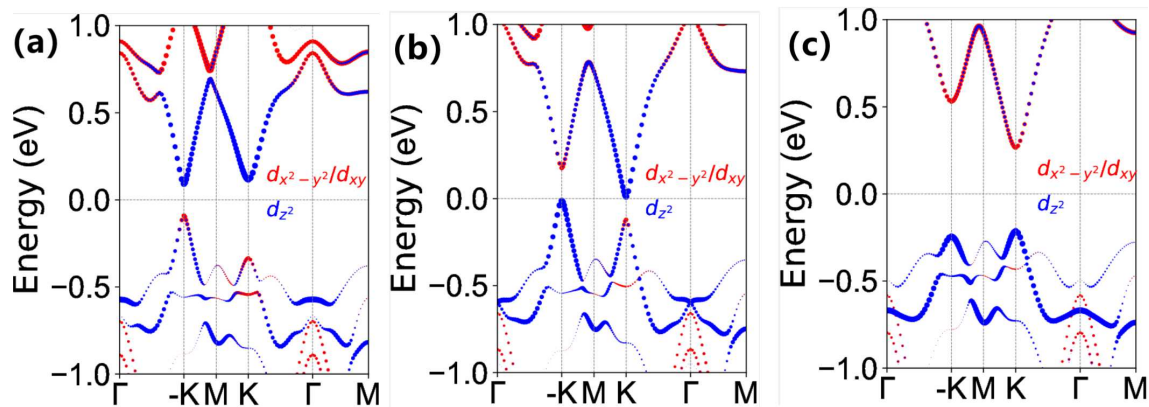


FIG. 4. (Color online) For out-of-plane magnetic anisotropy, the Ru- $d_{x^2-y^2}/d_{xy}$  and  $d_{z^2}$ -orbital characters of energy bands of monolayer RuBr<sub>2</sub> with  $U = 1.5$  eV (a), 2.0 eV (b) and 2.5 eV (c).

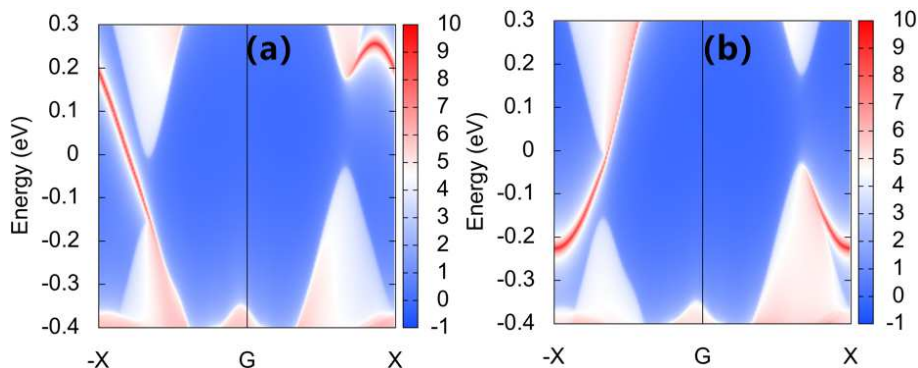


FIG. 5. (Color online) For RuBr<sub>2</sub> monolayer with out-of-plane magnetic anisotropy, the topological left (a) and right (b) edge states calculated along the (100) direction with  $U$  being 2.00 eV.

erties of RuBr<sub>2</sub> monolayer are investigated. Due to  $P\bar{6}m2$  space group, there are two independent elastic constants:  $C_{11}$  and  $C_{12}$ , and the corresponding values are 40.29 Nm<sup>-1</sup> and 14.57 Nm<sup>-1</sup> by using GGA. The calculated elastic constants meet the Born criteria of mechanical stability<sup>53</sup>:  $C_{11} > 0$  and  $C_{11} - C_{12} > 0$ , indicating its mechanical stability. Due to hexagonal symmetry, the Young's moduli  $C^{2D}$ , shear modulus  $G^{2D}$  and Poisson's ratios  $\nu^{2D}$  of RuBr<sub>2</sub> monolayer all are mechanically isotropic, and the calculated results show that they are 35.02 Nm<sup>-1</sup>, 12.86 Nm<sup>-1</sup> and 0.362, respectively.

#### IV. ELECTRONIC CORRELATION EFFECTS

Electronic correlations have significant impact on the magnetic, topological and electronic properties of 2D materials<sup>16,40,41</sup>. The direction of magnetic anisotropy can affect the symmetry of 2D materials, and then produce important influence on the electronic and topological properties<sup>40,41,54</sup>. Firstly, the magnetocrystalline direction of RuBr<sub>2</sub> monolayer is assumed to be along the out-of-plane one in considered  $U$  range (0-3 eV). The out-of-plane magnetic anisotropy allows a nonvanishing

Chern number of 2D materials with varied  $U$ <sup>54</sup>. The electronic structures of RuBr<sub>2</sub> monolayer with different  $U$  are calculated by GGA+SOC+ $U$ . The energy band structures at some representative  $U$  values are plotted in FIG.1 of electronic supplementary information (ESI), and the evolutions of energy band gaps vs  $U$  are plotted in Figure 3, along with the gaps at -K and K points.

For  $U < 1.8$  eV, the gap firstly increases, and then decreases, which is due to the transformation of valence band maximum (VBM). At small  $U$ , the RuBr<sub>2</sub> monolayer is an indirect gap semiconductor. The conduction band minimum (CBM) is at the -K point, whereas the VBM occurs at the one point being close to M point. With increasing  $U$ , the system becomes a direct gap semiconductor with both VBM and CBM being at -K point. Around the  $U = 1.8$  eV, the HVM with conduction electrons being intrinsically 100% valley polarized<sup>16</sup> can be achieved, whose gap at -K point gets closed, and a band gap of 0.31 eV still holds at K point. When the  $U$  reaches 2.105 eV, the other HVM state can be observed, where the -K valley holds the energy band gap (0.31 eV) and the K valley is metallic, opposite to the previous case. Between  $U = 1.8$  eV and 2.105 eV, the gap of about 26 meV can be observed, which is larger than the thermal energy



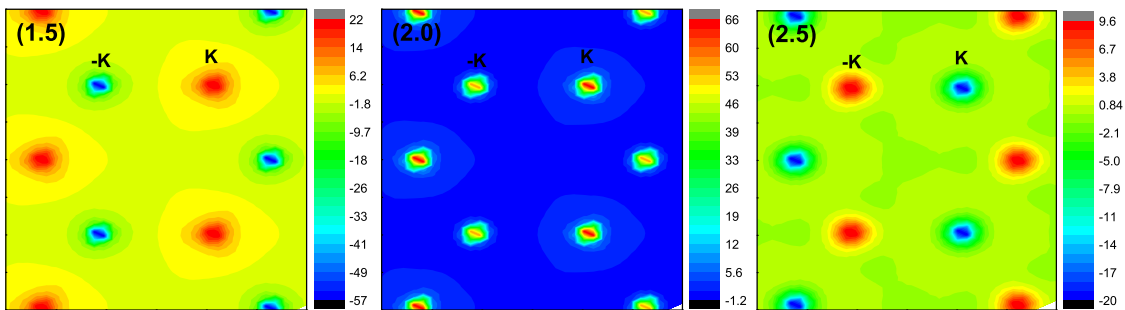


FIG. 6. (Color online) For RuBr<sub>2</sub> monolayer with out-of-plane magnetic anisotropy, the calculated Berry curvature distribution in the 2D Brillouin zone with different  $U$  (1.5 eV, 2.0 eV and 2.5 eV).

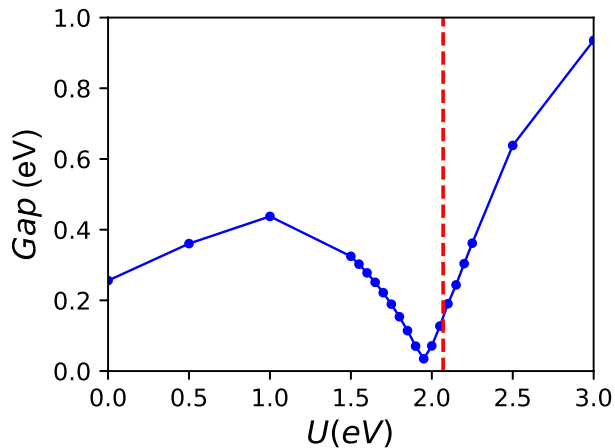


FIG. 7. (Color online) For RuBr<sub>2</sub> monolayer with in-plane magnetic anisotropy, the energy band gap as a function of  $U$  (0-3 eV). The vertical red dotted line means that actual MAE changes from out-of-plane to in-plane.

of room temperature (25 meV). However, for  $U > 2.105$  eV, the gap increases with increasing  $U$ , and the RuBr<sub>2</sub> monolayer changes from a direct gap semiconductor to an indirect gap semiconductor with CBM always being at K point.

In all regions, RuBr<sub>2</sub> monolayer is a FV material. The valley polarization can be observed in both valence and conduction bands at the -K and K points, and the corresponding valley splitting is plotted in FIG.2 of ESI. For  $U < 1.8$  eV, a remarkable valley splitting appears in the valence bands. However, for  $U > 2.105$  eV, the noteworthy valley polarization can be observed in the conduction bands. Between  $U = 1.8$  eV and 2.105 eV, with increasing  $U$ , the valley splitting in the valence bands decreases, and increases for the conduction bands. These can be understood by the transformation of Ru- $d$ -orbital characters of energy bands. In all  $U$  region, the  $d_{z^2}$  or  $d_{x^2-y^2}/d_{xy}$  orbitals of Ru atoms dominate the -K and K valleys of both valence and conduction bands. At representative  $U$  (1.5 eV, 2.0 eV and 2.5 eV), the Ru- $d_{x^2-y^2}/d_{xy}$  and  $d_{z^2}$ -orbital characters of energy bands of monolayer RuBr<sub>2</sub> are plotted in Figure 4. For  $U < 1.8$  eV, the  $d_{x^2-y^2}$  and

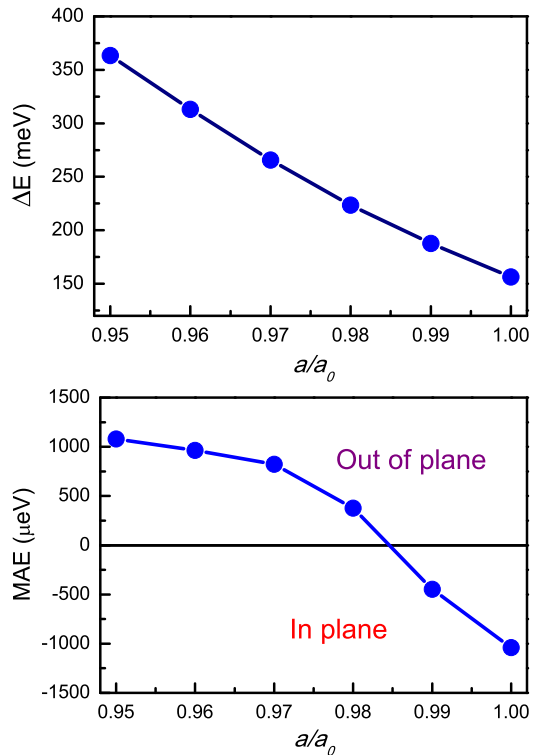


FIG. 8. (Color online) For RuBr<sub>2</sub> monolayer, the energy differences  $\Delta E$  with rectangle supercell between AFM and FM ordering and MAE as a function of strain  $a/a_0$ .

$d_{xy}$  orbitals dominate -K and K valleys in valence bands, and the  $d_{z^2}$  orbitals play a leading role for those in the conduction bands (see Figure 4 (a)). For  $U > 2.105$  eV, the situation is opposite to the previous case of  $U < 1.8$  eV for the distribution of Ru- $d$ -orbitals (see Figure 4 (c)).

The SOC induces valley polarization, which is contributed by the intra-atomic interaction:

$$\hat{H}_{SOC} = \lambda \hat{L} \cdot \hat{S} = \hat{H}_{SOC}^0 + \hat{H}_{SOC}^1 \quad (1)$$

where  $\lambda$ ,  $\hat{L}$  and  $\hat{S}$  are the coupling strength, the orbital angular momentum and spin angular momentum, respectively. Due to the magnetic exchange interaction, the  $\hat{H}_{SOC}^0$

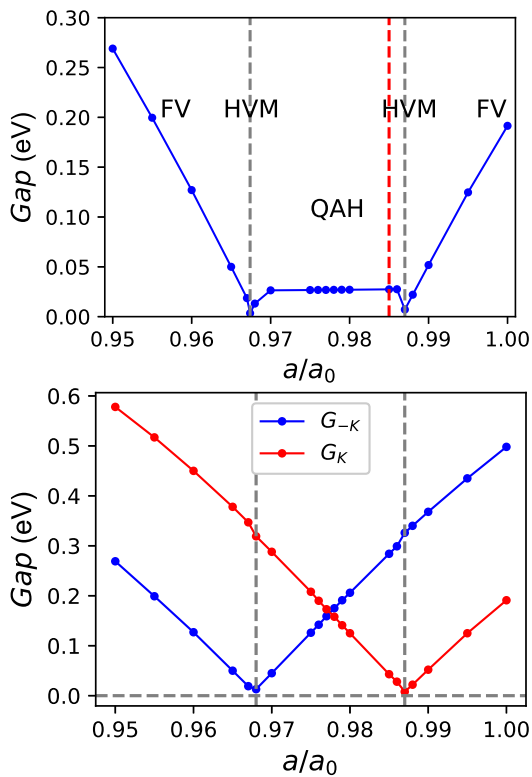


FIG. 9. (Color online) For RuBr<sub>2</sub> monolayer with out-of-plane magnetic anisotropy, the top plane shows global energy band gap as a function of strain  $a/a_0$  (0.95-1.00), and the phase diagram is shown with different strain region. The bottom plane shows the energy band gaps for the -K and K valleys. The vertical red dotted line means that actual MAE changes from out-of-plane to in-plane.

dominates the  $\lambda \hat{L} \cdot \hat{S}$ . For out-of-plane magnetization, the  $\hat{H}_{SOC}^0$  can be expressed as:

$$\hat{H}_{SOC}^0 = \alpha \hat{L}_z \quad (2)$$

The orbital basis for -K and K valleys with the group symmetry being  $C_{3h}$  can be written as<sup>12,14,15</sup>:

$$|\phi^\tau \rangle = \sqrt{\frac{1}{2}} (|d_{x^2-y^2} \rangle + i\tau |d_{xy} \rangle) \quad (3)$$

or

$$|\phi^\tau \rangle = |d_{z^2} \rangle$$

in which the subscript  $\tau$  represent valley index ( $\tau = \pm 1$ ). At K and -K valleys, the resulting energy can be expressed as:

$$E^\tau = \langle \phi^\tau | \hat{H}_{SOC}^0 | \phi^\tau \rangle \quad (4)$$

If the -K and K valleys are dominated by  $d_{x^2-y^2}$  and  $d_{xy}$  orbitals, the valley splitting  $|\Delta E|$  can be expressed as:

$$|\Delta E| = E^K - E^{-K} = 4\alpha \quad (5)$$

For the  $d_{z^2}$  orbitals, the valley splitting  $|\Delta E|$  is given as:

$$|\Delta E| = E^K - E^{-K} = 0 \quad (6)$$

If considering  $\hat{H}_{SOC}^1$ , the valley splitting  $|\Delta E|$  at K and -K valleys mainly from the  $d_{z^2}$  orbitals is not equal to zero. These can explain  $U$  dependence of valley splitting for conduction or valence bands.

When  $U$  is between 1.8 eV and 2.105 eV, the  $d_{x^2-y^2}$  and  $d_{xy}$  orbitals dominate the -K valley in the conduction bands and K valley in the valence band, and the  $d_{z^2}$  orbitals dominate -K valley in the valence bands and K valley in the conduction band (see Figure 4 (b)). This is a transitional region to achieve the changes of distribution of Ru- $d$ -orbitals with  $U < 1.8$  eV to  $U > 2.105$  eV. In other words, it can be seen that the band inversion of  $d_{xy}/d_{x^2-y^2}$  and  $d_{z^2}$  orbitals occurs at -K valley with  $U$  across 1.8 eV, and the band inversion appears again with  $U$  crossing 2.105 eV. It is noted that the gap of RuBr<sub>2</sub> monolayer closes, reopens, and then closes. The band inversion and novel change of gap suggest some topological phase transitions, and QAH insulator phases may exist between the two HVM states. Similar phenomenon can be observed in FeCl<sub>2</sub> and FeClF monolayers<sup>16,41</sup>. The chiral edge states are calculated to confirm QAH phases, which are plotted in Figure 5 with  $U=2.00$  eV. A chiral edge state does exist for left/right edge, which connects the conduction bands and valence bands. The Chern number is equal to one ( $C=1$ ) due to a single chiral edge state. The  $C=1$  can also be obtained by integrating the Berry curvature (see Figure 6) within the first Brillouin zone of RuBr<sub>2</sub> monolayer, which is consistent with a single gapless chiral edge band. It is clearly seen that a valley structure for both conduction and valence bands can coexist with QAH phase (See FIG.1 of ESI), and the K/-K valley can be polarized with the Fermi level into conduction/valence bands. That is also called VQAHI, which can combine valleytronics and spintronics with nontrivial band topology. With increasing  $U$ , the RuBr<sub>2</sub> monolayer can undergo the FV, HVM, QAH, HVM and FV states.

These electronic state transitions are related with the variation of Berry curvature. In considered  $U$  range, the Berry curvature is calculated, which is shown in Figure 6 at representative  $U$  values ( $U=1.5, 2.0$  and  $2.5$  eV). In all considered  $U$  range, the hot spots of Berry curvature are around -K and K valleys. For  $U < 1.8$  eV and  $U > 2.105$  eV, the Berry curvatures around two valleys have opposite signs and different magnitudes. However, for  $1.8 \text{ eV} < U < 2.105 \text{ eV}$ , they have the same signs. With increasing  $U$ , a topological phase transition is produced, which is connected by the first HVM state. In this transition, the sign of Berry curvature at -K valley flips. For example, the negative Berry curvature (-K valley) at  $U=1.5$  eV changes into positive one at  $U=2.0$  eV. When  $U$  continues to increase (The  $U$  spans the 2.105 eV), another topological phase transition induces the sign flipping of Berry curvature at K valley. For instance, the positive Berry curvature of K valley at  $U=2.0$  eV changes into negative one at  $U=2.5$  eV. These mean that the electronic correlation effects can induce sign-reversible Berry curvature, which is related with topological phase tran-

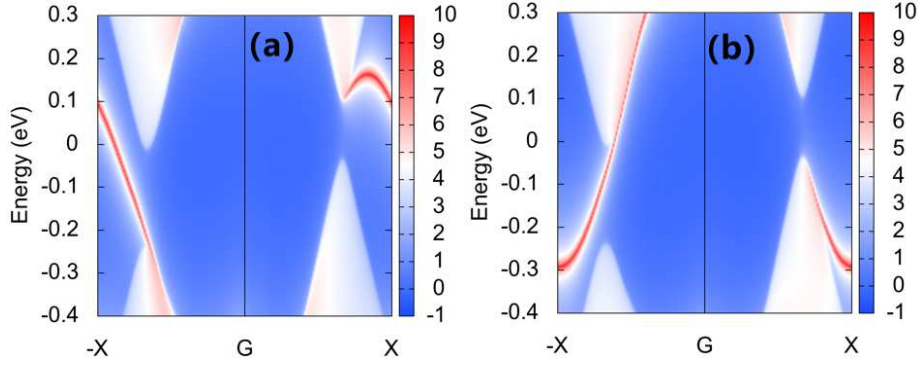


FIG. 10. (Color online) For RuBr<sub>2</sub> monolayer with out-of-plane magnetic anisotropy, the topological left (a) and right (b) edge states calculated along the (100) direction with  $a/a_0$  being 0.975.

sition.

Next, we assume that the magnetocrystalline direction of RuBr<sub>2</sub> monolayer is in-plane. By using GGA+SOC, the energy band gaps as a function of  $U$  are plotted in Figure 7, and the representative energy band structures are shown in FIG.3 of ESI. With increasing  $U$ , the gap firstly decreases, and reduces to zero (about  $U=1.95$  eV), and increases again. It is clearly seen that no QAH region appears, and no observable valley polarization in both the valence and conduction bands exists. Calculated results show that the distributions of Ru- $d$ -orbital characters are akin to the cases of out-of-plane, and the sign-reversible Berry curvature can also be observed, when  $U$  increases across about 1.95 eV. The hot spots of Berry curvature around two valleys have opposite signs and almost the same magnitudes. According to calculated results in Figure 2, the magnetocrystalline direction of RuBr<sub>2</sub> monolayer is out-of-plane with  $U$  being less than 2.07 eV, and is in-plane with  $U$  being greater than 2.07 eV. For  $U < 2.07$  eV, there can be FV, HVM and QAH states. However, only common FM semiconductors can exist with  $U > 2.07$  eV. As long as the actual  $U$  is between 1.8 eV and 2.07 eV, the RuBr<sub>2</sub> monolayer intrinsically is a VQAH.

## V. STRAIN EFFECTS

For a given material, the correlation strength  $U$  should be fixed, and should be determined from experiment. The competition between kinetic and interaction energies determines the strength of electronic correlation<sup>40</sup>. The strain can modify the distance between atoms, which can tune kinetic and interaction energies. For hexagonal lattice with a formula of MX<sub>2</sub>, by means of a low energy  $k \cdot p$  model analysis, a mechanism of producing VQAH via strain engineering is proposed, and a general picture of valley-contrasted band inversion is developed<sup>55</sup>. Then the effective Hamiltonian from strain contribution can be written as<sup>55</sup>:

$$H_\epsilon = \frac{D(\epsilon_{xx} + \epsilon_{yy})\hat{s}_0\hat{\sigma}_z}{2} = \frac{D\epsilon_{xx}\hat{s}_0\hat{\sigma}_z}{2} \quad (7)$$

where  $D$  and  $\epsilon_{xx}/\epsilon_{yy}$  are deformation potential and strain along x/y axis,  $\hat{s}_0$  and  $\hat{\sigma}_z$  denote the Pauli matrices. The  $H_\epsilon$  can induce band inversion, producing QAH phase.

Therefore, the RuBr<sub>2</sub> monolayer can be tuned into FV, HVM and QAH states, even though the actual  $U$  is larger than 2.07 eV. We use  $U=2.25$  eV as a example to prove the assumption, where the RuBr<sub>2</sub> monolayer is a common FM semiconductor. The  $a/a_0$  is used to simulate the biaxial strain, in which  $a$  and  $a_0$  are the strained and unstrained lattice constants. Here, the compressive strain ( $a/a_0 < 1$ ) is applied to achieve the transition of electronic states. To confirm the FM ground states, the total energy differences between AFM and FM ordering by using rectangle supercell are calculated as a function of  $a/a_0$ , as shown in Figure 8. In considered strain range, the FM states are always the magnetic ground states, and the compressive strain can enhance FM interaction, improving  $T_C$  of RuBr<sub>2</sub> monolayer.

Firstly, we assume that the magnetocrystalline direction of RuBr<sub>2</sub> monolayer is along the out-of-plane one. At some representative  $a/a_0$ , the energy band structures are plotted in FIG.4 of ESI, and the energy band gaps along with the gaps at -K and K valleys as a function of  $a/a_0$  are shown in Figure 9. For  $a/a_0 > 0.987$ , the gap decreases with increasing compressive strain. Around the  $a/a_0=0.987$ , the first HVM can be achieved, whose gap at K point gets closed. When the  $a/a_0$  reduces to 0.968, the other HVM state can be observed, where the -K valley is metallic, opposite to the previous case. Between  $a/a_0=0.987$  and 0.968, there is a gap of about 27 meV, which is close to the thermal energy of room temperature. For  $a/a_0 < 0.968$ , the gap increases with increasing compressive strain. In considered strain range, RuBr<sub>2</sub> monolayer is always a FV material, which can be confirmed by valley splitting in FIG.5 of ESI. For  $a/a_0 < 0.968$ , a remarkable valley splitting can be observed in the valence bands, while the noteworthy valley polarization exists in the conduction bands for  $a/a_0 > 0.987$ . Between  $a/a_0=0.968$  and 0.987, with increasing compressive strain, the valley splitting in the valence bands increases, and decreases for the conduction bands. These can also

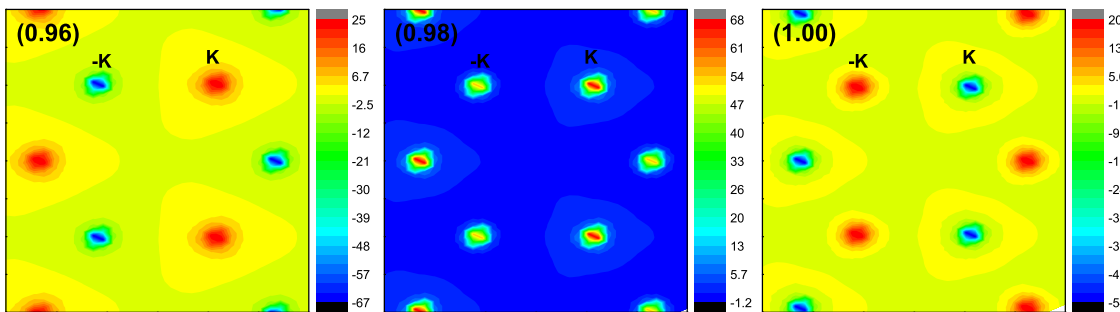


FIG. 11. (Color online) For RuBr<sub>2</sub> monolayer with out-of-plane magnetic anisotropy, the calculated Berry curvature distribution in the 2D Brillouin zone with different  $a/a_0$  (0.96, 0.98 and 1.00).

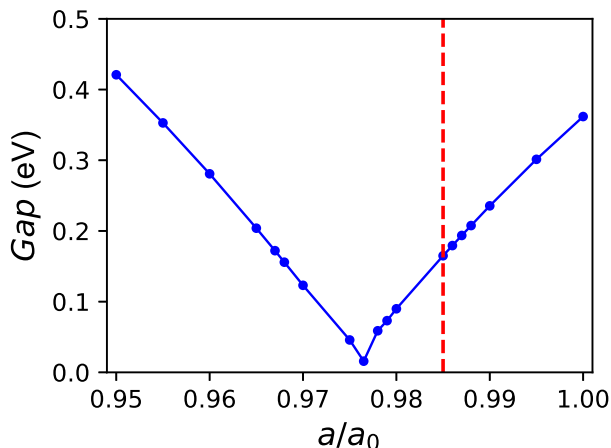


FIG. 12. (Color online) For RuBr<sub>2</sub> monolayer with in-plane magnetic anisotropy, the energy band gap as a function of strain  $a/a_0$  (0.95-1.00). The vertical red dotted line means that actual MAE changes from out-of-plane to in-plane.

be explained by the transformation of Ru- $d$ -orbital characters of energy bands with variational  $a/a_0$ , being analogous to changed  $U$ .

With increasing compressive strain, the gap of RuBr<sub>2</sub> monolayer gets closed, reopens, and then closes, which suggests that QAH insulator phases may exist between the two HVM states. To confirm QAH phases, the chiral edge states are plotted in Figure 10 at  $a/a_0=0.975$ . It is clearly seen that a chiral edge state for left/right edge connects the conduction bands and valence bands, which means that the Chern number is equal to one ( $C=1$ ). The VQAH can also be observed between the two HVM states. With increasing compressive strain, the RuBr<sub>2</sub> monolayer changes from FV to HVM to QAH to HVM to FV state. The sign-reversible Berry curvature can also be observed with increasing compressive strain, which is plotted in Figure 11 at representative  $a/a_0$  values. Similar phenomenon can be found in monolayer VSi<sub>2</sub>N<sub>4</sub><sup>56</sup>. With reduced  $a/a_0$ , the sign of Berry curvature at K valley firstly flips at about  $a/a_0=0.987$ , and then the Berry curvature at -K valley change sign at about  $a/a_0=0.968$ . These topological phase transitions are also related with

the band inversion of  $d_{xy}/d_{x^2-y^2}$  and  $d_{z^2}$  orbitals, being similar to varied  $U$ .

Next, the magnetocrystalline direction of RuBr<sub>2</sub> monolayer is supposed to be in-plane. The energy band gaps vs  $a/a_0$  are plotted in Figure 12, and the representative energy band structures are plotted in FIG.6 of ESI. With increasing compressive strain, the gap firstly decreases, and then increases. The corresponding critical  $a/a_0$  is about 0.976. There is not QAH phases and observable valley polarization in both the valence and conduction bands. The MAE vs  $a/a_0$  is calculate to determine intrinsic magnetic anisotropy of RuBr<sub>2</sub> monolayer, which is plotted in Figure 8. Based on calculated results, the magnetocrystalline direction of RuBr<sub>2</sub> monolayer is in plane with  $a/a_0$  being larger than 0.985, and is out-of-plane with  $a/a_0$  being less than 0.985. For  $a/a_0 < 0.985$ , there can be QAH, HVM and FV states. However, for  $a/a_0 > 0.985$ , there is only common FM semiconductor. The VQAH can indeed be achieved by strain, which possesses intrinsic PMA, QAH state and spontaneous valley splitting.

## VI. CURIE TEMPERATURE

Both electronic correlation effects ( $U$ ) and compressive strain ( $a/a_0$ ) can effectively tune the strength of FM interaction, which can produce important effects on Curie temperature  $T_C$  of monolayer RuBr<sub>2</sub>. The  $T_C$  is estimated at representative  $U$  (1.0 and 2.5 eV) and  $a/a_0$  (1.0 and 0.95) values with the Wolf algorithm based on the Heisenberg model, which can be expressed as:

$$H = -J \sum_{i,j} S_i \cdot S_j - A \sum_i (S_i^z)^2 \quad (8)$$

in which  $S_i/S_j$  and  $S_i^z$  are the spin vectors of each Ru atom and the spin component parallel to the  $z$  direction, and  $J$  and  $A$  are the nearest neighbor exchange parameter and MAE. The  $J$  with normalized spin vector ( $|S|=1$ ) can be attained by comparing energies of the AFM ( $E_{AFM}$ ) and FM ( $E_{FM}$ ) configurations with rectangle supercell, and the corresponding  $J$  can be written



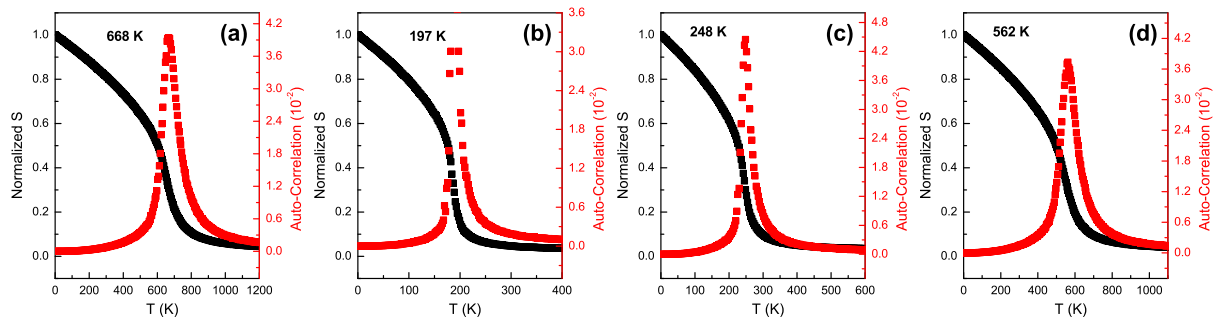


FIG. 13. (Color online) For RuBr<sub>2</sub> monolayer, the normalized magnetic moment ( $S$ ) and auto-correlation as a function of temperature with  $U=1.0$  eV (a), 2.5 eV (b) and  $a/a_0=1.0$  (c), 0.95 (d) at  $U=2.25$  eV.

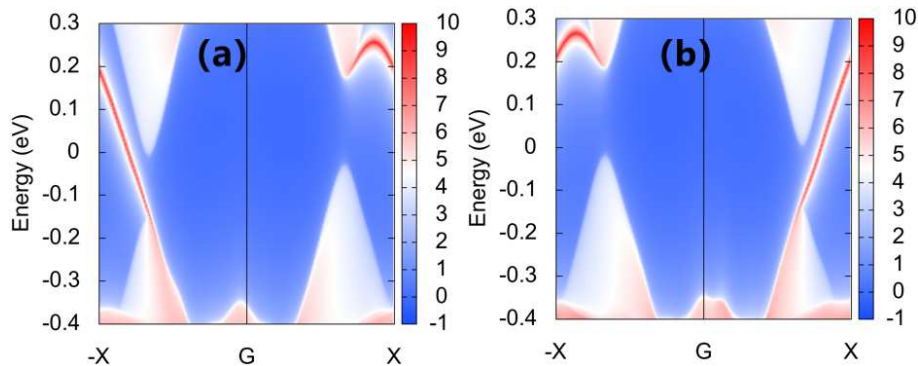


FIG. 14. (Color online) For RuBr<sub>2</sub> monolayer with out-of-plane magnetic anisotropy ( $U=2.0$  eV), the topological left edge states calculated along the (100) direction with SOC for magnetic moment of Ru along the positive (a) and negative (b)  $z$  direction, respectively.

as:

$$J = \frac{E_{AFM} - E_{FM}}{8} \quad (9)$$

The calculated normalized  $J$  are 53.67 meV and 13.95 meV for  $U=1.0$  eV and 2.5 eV, and are 19.55 meV and 45.41 meV at  $a/a_0=1.0$  and 0.95 with  $U=2.25$  eV. The normalized magnetic moment and auto-correlation vs temperature at representative  $U$  (1.0 and 2.5 eV) and  $a/a_0$  (1.0 and 0.95) values are plotted in Figure 13, and the predicted  $T_C$  is about 668/197 K for  $U=1.0/2.5$  eV, and 248/562 K for  $a/a_0=1.0/0.95$ . So, it is very key for estimating  $T_C$  to use reasonable  $U$ . It is found that the compressive strain can improve  $T_C$ .

## VII. DISCUSSION AND CONCLUSION

The novel electronic state of RuBr<sub>2</sub> monolayer, like FV, HVM and QAH states, depends on  $U$ , which should be determined from experiment result. However, novel electronic state can also be achieved from common one by strain. That is to say, the FV, HVM and QAH states can indeed be realized in RuBr<sub>2</sub> monolayer. These analysis and results can be readily extended to monolayer MXY ( $M = \text{Ru, Os}$ ;  $X/Y = \text{Cl, Br I}$ ). The VQAH uniquely combines valleytronics and spintronics with nontrivial band

topology, which needs appropriate energy band gap and valley splitting for the practical application. For RuBr<sub>2</sub> monolayer, the band gap of VQAH is about 26 meV (see Figure 3 and Figure 9), and the valley splitting can simultaneously be larger than 100 meV by choosing appropriate  $U$  or  $a/a_0$  (see FIG.2 and FIG.5 of ESI). These values are higher than the thermal energy of room temperature (25 meV), which makes for room temperature applications. The VQAH has a very special behavior of the chiral-spin-valley locking for the edge state. Taking unstrained RuBr<sub>2</sub> with  $U=2.0$  eV as a example, the topological left edge states for magnetic moment of Ru along the positive and negative  $z$  direction are plotted in Figure 14. The valley polarization for bulk can be switched by reversing the magnetization direction with magnetic moment of Ru along the negative  $z$  direction. Due to the bands all dominated by spin-down bands near the Fermi level, the edge state shown in Figure 14 (a) is also spin down with 100% spin polarization and 100% valley polarization. For the  $-K$  and  $K$  valleys, the edge state only appears at the  $-K$  valley, which is due to the flipping of the sign of the Berry curvature or band inversion at  $-K$  valley. When the magnetization is reversed, the edge state shown in Figure 14 (b) moves to the  $K$  valley, which has an opposite spin direction and chiral.

In summary, we have demonstrated the possibility of

realizing VQAHI in RuBr<sub>2</sub> monolayer, as a representative of the monolayer MXY (M = Ru, Os; X/Y=Cl, Br I). The varied  $U$  can tune interplay among magnetic, correlation and SOC, which can result in different electronic state, like FV, HVM and QAH states. The VQAHI can be achieved between two HVM states, which possesses exotic chiral-spin-valley locking edge states. It is found that strain is an effective method to achieve VQAHI from a common FM semiconductor. These topological phase transitions are related with sign-reversible Berry curvature and band inversions of  $d_{xy}/d_{x^2-y^2}$  and  $d_{z^2}$  orbitals at -K and K valleys. It is found that correlation strength and strain can observably tune magnetic interaction, which is related with Curie temperature. Our works provide a comprehensive understanding of RuBr<sub>2</sub> monolayer, which can be used as a candidate material

with complete spin and valley polarization, combining valleytronics, spintronics and topological electronics.

## ACKNOWLEDGMENTS

This work is supported by Natural Science Basis Research Plan in Shaanxi Province of China (2021JM-456) and Graduate Innovation Fund Project in Xi'an University of Posts and Telecommunications (CXJJDL2021001). We are grateful to the Advanced Analysis and Computation Center of China University of Mining and Technology (CUMT) for the award of CPU hours and WIEN2k/VASP software to accomplish this work.

- 
- <sup>1</sup> J. R. Schaibley, H. Yu, G. Clark, P. Rivera, J. S. Ross, K. L. Seyler, W. Yao, and X. Xu, *Nat. Rev. Mater.* **1**, 16055 (2016).
  - <sup>2</sup> S. A. Vitale, D. Nezich, J. O. Varghese, P. Kim, N. Gedik, P. Jarillo-Herrero, D. Xiao, and M. Rothschild, *Small* **14**, 1801483 (2018).
  - <sup>3</sup> D. Xiao, G. B. Liu, W. Feng, X. Xu, and W. Yao, *Phys. Rev. Lett.* **108**, 196802 (2012).
  - <sup>4</sup> D. Xiao, W. Yao, and Q. Niu, *Phys. Rev. Lett.* **99**, 236809 (2007).
  - <sup>5</sup> G. Pacchioni, *Nat. Rev. Mater.* **5**, 480 (2020).
  - <sup>6</sup> W. Yao, D. Xiao, and Q. Niu, *Phys. Rev. B* **77**, 235406 (2008).
  - <sup>7</sup> C. Zhao, T. Norden, P. Zhang, P. Zhao, Y. Cheng, F. Sun, J. P. Parry, P. Taheri, J. Wang, Y. Yang, T. Scrace, K. Kang, S. Yang, G. Miao, R. Sabirianov, G. Kioseoglou, W. Huang, A. Petrou and H. Zeng, *Nat. Nanotechnol.* **12**, 757 (2017).
  - <sup>8</sup> H. Zeng, J. Dai, W. Yao, D. Xiao and X. Cui, *Nat. Nanotechnol.* **7**, 490 (2012).
  - <sup>9</sup> D. MacNeill, C. Heikes, K. F. Mak, Z. Anderson, A. Kormányos, V. Zólyomi, J. Park and D. C. Ralph, *Phys. Rev. Lett.* **114**, 037401 (2015).
  - <sup>10</sup> D. Xiao, M. C. Chang, and Q. Niu, *Rev. Mod. Phys.* **82**, 1959 (2010).
  - <sup>11</sup> M. Zeng, Y. Xiao, J. Liu, K. Yang and L. Fu, *Chem. Rev.* **118**, 6236 (2018).
  - <sup>12</sup> W. Y. Tong, S. J. Gong, X. Wan, and C. G. Duan, *Nat. Commun.* **7**, 13612 (2016).
  - <sup>13</sup> X. R. Kong, L. Y. Li, L. B. Liang, F. M. Peeters and X. J. Liu, *Appl. Phys. Lett.* **116**, 192404 (2020).
  - <sup>14</sup> P. Zhao, Y. Dai, H. Wang, B. B. Huang and Y. D. Ma, *ChemPhysMater*, **1**, 56 (2022).
  - <sup>15</sup> R. Li, J. W. Jiang, W. B. Mi and H. L. Bai, *Nanoscale* **13**, 14807 (2021).
  - <sup>16</sup> H. Hu, W. Y. Tong, Y. H. Shen, X. Wan, and C. G. Duan, *npj Comput. Mater.* **6**, 1 (2020).
  - <sup>17</sup> S. D. Guo, J. X. Zhu, W. Q. Mu and B. G. Liu, *Phys. Rev. B* **104**, 224428 (2021).
  - <sup>18</sup> S. D. Guo, X. S. Guo, X. X. Cai and B. G. Liu, *Phys. Chem. Chem. Phys.* **24**, 715 (2022).
  - <sup>19</sup> J. Zhou, Y. P. Feng, and L. Shen, *Phys. Rev. B* **102**, 180407(R) (2020).
  - <sup>20</sup> P. Zhao, Y. Ma, C. Lei, H. Wang, B. Huang, and Y. Dai, *Appl. Phys. Lett.* **115**, 261605 (2019).
  - <sup>21</sup> R. Peng, Y. Ma, X. Xu, Z. He, B. Huang, and Y. Dai, *Phys. Rev. B* **102**, 035412 (2020).
  - <sup>22</sup> Z. Song, X. Sun, J. Zheng, F. Pan, Y. Hou, M. H. Yung, J. Yang, and J. Lu, *Nanoscale* **10**, 13986 (2018).
  - <sup>23</sup> X. Y. Feng, X. L. Xu, Z. L. He, R. Peng, Y. Dai, B. B. Huang and Y. D. Ma, *Phys. Rev. B* **104**, 075421 (2021).
  - <sup>24</sup> Y. B. Liu, T. Zhang, K. Y. Dou, W. H. Du, R. Peng, Y. Dai, B. B. Huang, and Y. D. Ma, *J. Phys. Chem. Lett.* **12**, 8341 (2021).
  - <sup>25</sup> W. Du, Y. Ma, R. Peng, H. Wang, B. Huang, and Y. Dai, *J. Mater. Chem. C* **8**, 13220 (2020).
  - <sup>26</sup> Y. Zang, Y. Ma, R. Peng, H. Wang, B. Huang, and Y. Dai, *Nano Res.* **14**, 834 (2021).
  - <sup>27</sup> C. L. Kane and E. J. Mele, *Phys. Rev. Lett.* **95**, 226801 (2005).
  - <sup>28</sup> C. L. Kane and E. J. Mele, *Phys. Rev. Lett.* **95**, 146802 (2005).
  - <sup>29</sup> C. Z. Chang, J. S. Zhang, X. Feng et al., *Science* **340**, 167 (2013).
  - <sup>30</sup> J. G. Checkelsky, J. T. Ye, Y. Onose et al., *Nat. Phys.* **8**, 729 (2012).
  - <sup>31</sup> Q. L. Sun, Y. D. Ma and N. Kioussis, *Mater. Horiz.* **7**, 2071 (2020).
  - <sup>32</sup> Y. Li, J. H. Li, Y. Li et al., *Phys. Rev. Lett.* **125**, 086401 (2020).
  - <sup>33</sup> S. D. Guo, W. Q. Mu, X. B. Xiao and B. G. Liu, *Nanoscale*, **13**, 12956 (2021).
  - <sup>34</sup> J. Zhou, Q. Sun, and P. Jena, *Phys. Rev. Lett.* **119**, 046403 (2017).
  - <sup>35</sup> L. Liu, B. Zhao, J. Y. Zhang et al., *Phys. Rev. B* **104**, 245414 (2021).
  - <sup>36</sup> M. Vila, J. H. Garcia and S. Roche, *Phys. Rev. B* **104**, L161113 (2021).
  - <sup>37</sup> R. K. Barik and A. K. Singh, *Chem. Mater.* **33**, 6311 (2021).
  - <sup>38</sup> X. C. Zhai and Y. M. Blanter, *Phys. Rev. B* **101**, 155425 (2020).
  - <sup>39</sup> H. Huan, Y. Xue, B. Zhao, G. Y. Gao, H. R. Bao and Z. Q. Yang, *Phys. Rev. B* **104**, 165427 (2021).

- <sup>40</sup> S. Li, Q. Q. Wang, C. M. Zhang, P. Guo and S. A. Yang, Phys. Rev. B **104**, 085149 (2021).
- <sup>41</sup> S. D. Guo, J. X. Zhu, M. Y. Yin and B. G. Liu, arXiv:2111.07110 (2021).
- <sup>42</sup> P. Hohenberg and W. Kohn, Phys. Rev. **136**, B864 (1964); W. Kohn and L. J. Sham, Phys. Rev. **140**, A1133 (1965).
- <sup>43</sup> G. Kresse, J. Non-Cryst. Solids **193**, 222 (1995).
- <sup>44</sup> G. Kresse and J. Furthmüller, Comput. Mater. Sci. **6**, **15** (1996).
- <sup>45</sup> G. Kresse and D. Joubert, Phys. Rev. B **59**, 1758 (1999).
- <sup>46</sup> J. P. Perdew, K. Burke and M. Ernzerhof, Phys. Rev. Lett. **77**, 3865 (1996).
- <sup>47</sup> A. A. Mostofia, J. R. Yatesb, G. Pizzif, Y.-S. Lee, I. Souzad, D. Vanderbilt and N. Marzarif, Comput. Phys. Commun. **185**, 2309 (2014).
- <sup>48</sup> Q. Wu, S. Zhang, H. F. Song, M. Troyer and A. A. Soluyanov, Comput. Phys. Commun. **224**, 405 (2018).
- <sup>49</sup> T. Fukui, Y. Hatsugai and H. Suzuki, J. Phys. Soc. Japan. **74**, 1674 (2005).
- <sup>50</sup> H. J. Kim, <https://github.com/Infant83/VASPBERRY>, (2018).
- <sup>51</sup> H. J. Kim, C. Li, J. Feng, J.-H. Cho, and Z. Zhang, Phys. Rev. B **93**, 041404(R) (2016).
- <sup>52</sup> L. Liu, X. Ren, J. H. Xie, B. Cheng, W. K. Liu, T. Y. An, H. W. Qin and J. F. Hu, Appl. Surf. Sci. **480**, 300 (2019).
- <sup>53</sup> E. Cadelano and L. Colombo, Phys. Rev. B **85**, 245434 (2012).
- <sup>54</sup> X. Liu, H. C. Hsu and C. X. Liu, Phys. Rev. Lett. **111**, 086802 (2013).
- <sup>55</sup> Z. L. He, R. Peng, Y. Dai, B. B. Huang and Y. D. Ma, Appl. Phys. Lett. **119**, 243102 (2021).
- <sup>56</sup> X. Zhou, R. Zhang, Z. Zhang, W. Feng, Y. Mokrousov and Y. Yao, npj Comput. Mater. **7**, 160 (2021).